Rich collision dynamics of soft and sticky crystalline nanoparticles: Numerical experiments

Yoichi Takato,* Michael E. Benson, and Surajit Sen†
Department of Physics, The State University of New York at Buffalo, Buffalo, New York 14260-1500
(Received 19 December 2014; revised manuscript received 12 July 2015; published 9 September 2015)

A molecular dynamics study on the collisional dynamics of soft and sticky single face-centered cubic crystal nanoparticles is presented. The softness and stickiness of the nanoparticles are controlled by varying parameters in the Lennard-Jones potential that is used to describe the interatomic interactions. Softening of nanoparticles due to extensive plastic deformations is observed as was previously found in hard nanoparticles. Further, two primary plastic deformation modes, slip and twinning, of the nanoparticles are found to play important roles in the temperature dependence of the coefficient of restitution. Additionally, we observe the effects of surface roughness, facets, and edges in the collisional behaviors of the sticky nanoparticles in low-velocity collisions. Nevertheless, the Johnson-Kendall-Roberts theory for macroscopic adhesive bodies still remains valid in nearly spherical nanoparticles.

DOI: 10.1103/PhysRevE.92.032403 PACS number(s): 62.20.F−, 36.40.−c, 45.50.Tn, 62.25.−g

I. INTRODUCTION

The use of nanoparticles is becoming increasingly prevalent and common in many areas. In the materials industries, nanoparticles are utilized to design and create functional materials. For instance, nanoparticle-reinforced composite materials attain an extra strength by virtue of the strong mechanical properties of the nanoparticles embedded in such composite materials (for example, Ref. [1]). The unique mechanical properties of the nanoparticles have been investigated because of their importance in various applications. The properties of nanoparticles often exhibit size dependence. In contrast, properties of bulk materials, in general, do not show size dependence. The yield strength of nanoparticles serves as an example of an important and intriguing size-dependent property. When nanoparticles are small, they have a yield strength that is higher than that of the corresponding bulk materials. This allows the small nanoparticles to withstand a high amount of external stress [2]. Additionally, high-yield strength is one of the many examples of the size-dependent properties of nanoparticles that has led to the recent increase in interest in and use of nanoparticles.

Crystal structure in nanosized materials is one of the key factors that influences how the materials deform. When crystal structured materials undergo permanent deformation at low strain rate, the materials often exhibit slip deformation and have favored directions and planes. In face-centered cubic (fcc) lattice materials there are four {111} slip planes and three ⟨110⟩ slip directions in a unit cell [3]. Small nanoparticles of a single fcc crystal colliding on the {100} faceted surfaces also show the slip deformation of the crystal in numerical simulations [4]. Once dislocations are nucleated, they propagate until reaching the free surface. Thus, the resultant deformations along with the slip planes formed in nanoparticles are extensive. Additionally, at higher strain rate, the nanoparticles deform in such a way that they become flattened and stretched in the directions perpendicular to the collision axis [4,5]. The nanoparticles at this velocity do not show apparent dislocations on the slip planes.

The adhesion of nanoparticles becomes progressively more significant as the size decreases due to their high surface-volume ratio. Therefore, nanoparticles tend to be sticky [6–9]. This adhesion is an important physical property for some applications. For instance, the deposition processes in nanocrystalline materials utilize adhesion in order to deposit nanoparticles on a substrate (for a review in Ref. [10]). In such a small length scale, the molecular dynamics (MD) method is frequently used as a tool to probe nanoscale adhesion phenomena [11–15]. In protoplanetary disk formation the van der Waals attractive interactions between small particles are one of the crucial driving forces behind dust aggregations [16–18]. In a study in astrophysics, large-scale MD simulations of adhesive nanoparticles with a hundred million atoms have been performed by Tanaka *et al.* [19]. They show that the contact force between the nanoparticles that collide at low velocities approaches the Johnson-Kendall-Roberts (JKR) force [20] as the nanoparticle size increases.

The coefficient of restitution (COR) defined as the ratio of rebound velocity v_{reb} to collision velocity v_{coll} ($e \equiv v_{\mathrm{reb}}/v_{\mathrm{coll}}$) quantifies the loss of the translational kinetic energy of a colliding system. The COR is used to demonstrate the collisional properties of the nanoparticles.

Nanoparticles in recent MD simulations were found to be very soft when they collide at high speeds above the yield point [4,9,21]. The softness is attributed to large translational kinetic energy loss during collision and is evidenced by the permanently and extensively deformed nanoparticles [4,21] and also by the incoming velocity-independent recoiling velocity [4,9]. The latter finding gives rise to the COR of the nanoparticles described by a power law: COR $e \propto v_{\mathrm{coll}}^{-1}$ [4,21], while the coefficient of restitution of macroscopic spheres is described by a different power law $e \propto v_{\mathrm{coll}}^{-1/4}$ [22,23]. However, the detailed mechanism of the softening that seems to contradict the existence of the super-hard nanoparticles is not well understood.

We present results of collision behaviors in two types of nearly spherical faceted nanoparticles that have different mechanical properties: soft nanoparticles and sticky nanoparticles. The soft nanoparticles refer to the nanoparticles described by the 9-6 Lennard-Jones (LJ) potential with no adhesion between nanoparticles. This potential yields softer mechanical

*ytakato@buffalo.edu
†sen@buffalo.edu

properties than the 12-6 LJ potential. The sticky nanoparticles refer to the nanoparticles described by the 12-6 LJ potential with adhesion between nanoparticles. We will present collision behaviors of those nanoparticles as follows.

In the high-speed collisions accompanied by plastic deformations, we found anomalous softening as was observed in hard nanoparticles described by coefficient of restitution $e \propto v_{\rm coll}^{-1}$ in both soft and sticky nanoparticles. Additionally, we saw permanent crystal structure changes occur either by slip at relatively low collision speed or by twinning at even higher collision speed. Deformation by slip is enhanced when temperature is increased, whereas deformation by twinning is not. Finally, we found that the chance of coalescence of sticky nanoparticles rises at higher collision velocity.

In low-speed collisions, it appears that the adhesion effect in the coefficient of restitution is consistent with JKR theory. Also, collisions on faceted surfaces at low speeds increase the chance of coalescence. We observed that viscoelasticity of nanoparticles is vanishingly small at low temperature but becomes more pronounced with increasing temperature.

II. METHODS

We perform classical MD simulations for a collinear collision between two identical approximately spherical nanoparticles of radius R. The nanoparticles are carved out of a block that is constituted of an fcc single crystal. Therefore, the resultant nanoparticles exhibit prominent facets and steps on their surface as exhibited in Fig. 1. The pairwise interatomic interaction for nanoparticles reported in this paper employs either the 12-6 LJ or the 9-6 LJ potentials.

Two mechanically different nanoparticles are prepared in our work: purely repulsive soft nanoparticles and sticky nanoparticles. While the softness of the nanoparticles is determined by the *intra*nanoparticle interaction, the repulsion and adhesion between two nanoparticles are determined by the *inter*nanoparticle interaction. Thus, we describe the interatomic potentials individually for internanoparticle and intrananoparticle interactions.

In regard to the *intra*nanoparticle interaction, that is, the interaction for the atoms that reside inside each nanoparticle, the 9-6 LJ potential described by Eq. (1) is utilized for the soft nanoparticle and the standard 12-6 LJ potential described by Eq. (2) with a prefactor $C = 1$ is chosen for the sticky nanoparticles. Both potentials are truncated at the cutoff distance $r_{c,1}$,$r_{c,2} = 2.5\sigma$ to make a balance between the computation time and the accuracy level of the collision simulations as discussed in Ref. [4]. They are shifted to zero at the cutoff distance by adding constant energies ϵ_1 and ϵ_2 to Eqs. (1) and (2), respectively. The shift eliminates the discontinuity that arises from the truncation, leading to reduced numerical error.

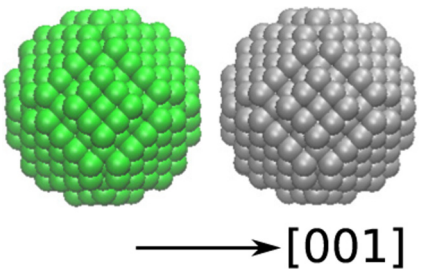

FIG. 1. (Color online) Nanoparticles that collide on their {100} facets.

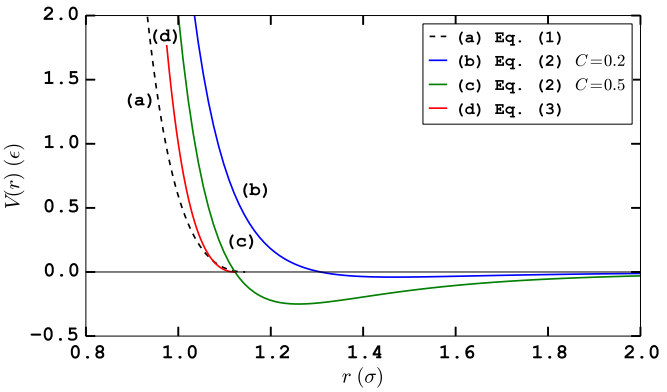

FIG. 2. (Color online) The interatomic potentials for *inter*nanoparticle interactions. Force $\mathbf{F}$ between atoms is determined by $\mathbf{F} = -\nabla V(r_{ij})$. From this definition, negative and positive slopes in the potential lead to repulsive and attractive forces, respectively. (a) Soft nanoparticle: Eq. (1). The gentle slope compared with the curve (d) makes the nanoparticles softer. The cutoff for this potential at $r_{c,2} = (3/2)^{1/3}\sigma$ results in repulsion. (b) Weakly attractive nanoparticle: Eq. (2) with $C = 0.2$. The graph of the potential shown as a curve (b) contains both the negative slope for small r_{ij} and the positive slope for large r_{ij}, which is essential to model sticky nanoparticles. (c) Strongly attractive nanoparticle: Eq. (2) with $C = 0.5$. (d) Hard nanoparticle in Ref. [4]: Eq. (3). The cutoff value $r_{c,3} = 2^{1/6}\sigma$ for atoms between two different nanoparticles makes them purely repulsive, illustrated as the purely negative slope.

Though the *inter*nanoparticle interaction, i.e., the interaction for atoms in different nanoparticles, is also described by the above-mentioned potentials, the cutoff distance takes a different value to impart repulsion between two nanoparticles during collision. The purely repulsive soft nanoparticles are modeled by the use of the 9-6 LJ potential in Eq. (1). It is truncated at its potential minimum $r_{c,1} = (3/2)^{1/3}\sigma$ in order to exclude the adhesion part of the potential at $r_{ij} > r_{c,1}$. It is also shifted to zero by adding ϵ_2 to get rid of the discontinuity at $r_{c,1}$. This purely repulsive potential is a variation of the Weeks-Chandler-Anderson (WCA) potential [24].

The sticky nanoparticle in the *inter*nanoparticle interaction employs a modified form of the 12-6 LJ potential as shown in Eq. (2) with $C \neq 1$. A cutoff distance $r_c = 2.5\sigma$ for internanoparticle atoms is used to make the nanoparticles sticky. By varying the C value in the range $0 < C < 1$ in Eq. (2) for the atoms in different nanoparticles, a desirable adhesion strength between the nanoparticles is achieved. This potential was originally introduced in Refs. [6,7] to model bouncy nanoparticles that occur in nanoparticle deposition processes. The curves (b) and (c) in Fig. 2 are the potentials with $C = 0.2$ and 0.5 for the weakly attractive nanoparticles and for the strongly attractive nanoparticles, respectively.

TABLE I. Nanoparticle (NP) types and parameters for the interatomic potentials.

	Eq. (k)	Internanoparticle		Intrananoparticle
Type	($k \in \{1,2,3\}$)	Interaction	$r_{c,k}$	$r_{c,k}$
Soft NP	(1)	Repulsive (modified WCA)	$(3/2)^{1/3}\sigma$	2.5σ
Sticky NP	(2)	Adhesive (modified LJ)	2.5σ	2.5σ
Hard NP (Ref. [4])	(3)	Repulsive (WCA)	$2^{1/6}\sigma$	2.5σ

For reference, a potential for the hard nanoparticles reported in Ref. [4] is written in Eq. (3). The potentials mentioned above are presented below:

$$V_{\text{soft}} = \begin{cases} 4\epsilon\left[\left(\frac{\sigma}{r_{ij}}\right)^9 - \left(\frac{\sigma}{r_{ij}}\right)^6\right] + \epsilon_1, & r_{ij} < r_{c,1} \\ 0 & r_{ij} \geqslant r_{c,1} \end{cases}, \quad (1)$$

$$V_{\text{sticky}} = \begin{cases} 4\epsilon\left[\left(\frac{\sigma}{r_{ij}}\right)^{12} - C\left(\frac{\sigma}{r_{ij}}\right)^6\right] + \epsilon_2, & r_{ij} < r_{c,2} \\ 0 & r_{ij} \geqslant r_{c,2} \end{cases}, \quad (2)$$

$$V_{\text{hard}} = \begin{cases} 4\epsilon\left[\left(\frac{\sigma}{r_{ij}}\right)^{12} - \left(\frac{\sigma}{r_{ij}}\right)^6\right] + \epsilon_3, & r_{ij} < r_{c,3} \\ 0 & r_{ij} \geqslant r_{c,3} \end{cases}. \quad (3)$$

The potentials and parameters to determine the mechanical properties are listed in Table I for the sake of clarity.

The time integration of the equations of motion with the potentials is carried out by the velocity Verlet algorithm and its time step dt is set to 1.08×10^{-14} s ($0.005\sqrt{m\sigma^2/\epsilon}$ in LJ unit). It should be noted that all the SI units used in this paper are computed from parameters of the 12-6 LJ potential for an argon atom [4].

All nanoparticles reported here are constituted of a single fcc crystal with no defects. Two identical nanoparticles are first equilibrated over 10 000 time steps in the canonical ensemble (Nosé-Hoover thermostat [25,26]) at temperature T. They are subsequently made to collide head-on at various collision velocities v_{coll} in the microcanonical ensemble. As illustrated in Fig. 1, the collision surface is chosen as {100} facets unless otherwise noted. The total energy of the system during the collision phase is maintained around 10^{-5} in relative error. Approximately 30 simulation runs are carried out at each collision velocity with different initial conditions for the ensemble average.

In the case of soft nanoparticles, the temperature of the nanoparticles is varied between $T = 2.4$ K and 21.6 K. The temperature range is chosen so that the smallest nanoparticle remains solid even though the melting temperature of nanoscale materials goes down as the size decreases [27,28]. The size of the soft nanoparticle ranges between number of atoms $N = 603$ ($R = 1.6$ nm) and 2093 ($R = 2.4$ nm).

In sticky nanoparticle simulations, the adhesive strength C introduced in the attractive part of Eq. (2) controls the stickiness of the nanoparticles. The strength C in our simulations is varied between 0.2 and 0.5 so that nanoparticles tend to bounce after collision. The sticky nanoparticles range between $N = 603$ ($R = 1.6$ nm) and 44 403 ($R = 7.1$ nm) in size. The temperature for all collisions of the sticky nanoparticles is set to $T = 2.4$ K.

Our MD simulations are carried out via LAMMPS [29]. Only for the sticky nanoparticles, we introduced a modification in the LAMMPS source code to achieve the above-mentioned adhesive strength C in Eq. (2). We use VMD [30] for visualization of the nanoparticles.

III. RESULTS

The velocity range of the colliding nanoparticles used in our simulations covers both elastic and plastic collision regimes. Collisional behaviors, often characterized by translational kinetic energy loss, depend strongly on deformation mechanisms. In low-speed impacts, energy loss arises from viscoelasticity and adhesion. In high-speed impacts, energy loss in the nanoparticles is primarily attributed to crystal structure changes. Such nanoparticles undergo either deformations by slip or by twinning, depending on strain rate and temperature. Generally, collisions resulting in crystal structure changes require more energy to deform than elastic collisions.

Thus, we will separately treat the two collision regimes. In Sec. III A, high-velocity collisions including plastic deformation modes will be presented. In Sec. III B, low-velocity collisions will be presented. In each section, soft nanoparticles and sticky nanoparticles will be discussed independently since these properties that are imparted to the nanoparticles by changing the potential parameters measurably affect their collision behaviors.

A. High-velocity collision

The dynamics and the behavior of the COR of the soft nanoparticles which collide at high speeds is discussed in subsection 1. In subsection 2, the sticky nanoparticles are dealt with for various adhesion strengths C.

1. *Soft nanoparticles*

In Fig. 3, the CORs of soft nanoparticles (modified WCA particles) of 603 atoms at several temperatures are shown. In this section, we focus on the CORs in the plastic collision regime where $v_{\text{coll}} > 80$ m/s. The plastic collision regime was identified by the appearance of surface dislocations after collision in the simulations [4]. The COR of the nanoparticles at temperature $T = 2.4$ K falls linearly in the plot and can thus be expressed by an approximate power of collision velocity, i.e., $e \propto v_{\text{coll}}^{-\alpha}$ with $\alpha \sim 1$. This expression of the COR of the soft nanoparticle remains the same as in our previous report [4] even if the softer potential described by Eq. (1) is adopted, though the COR at each velocity is reduced by the same rate in the entire velocity range.

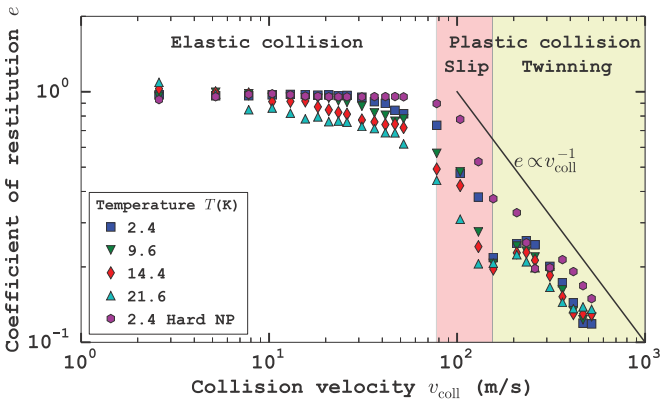

FIG. 3. (Color online) COR of soft nanoparticles of $N = 603$ atoms. Unshaded background ($v_{\rm coll} < 80$ m/s) represents elastic collision regime. Red shaded background (80 m/s $< v_{\rm coll} <$ 155 m/s) represents a plastic collision regime where the COR shows temperature dependence. Yellow shaded background (155 m/s $< v_{\rm coll}$) represents a plastic collision regime where the COR shows temperature independence.

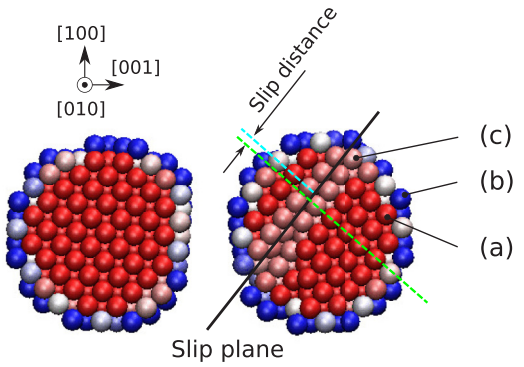

FIG. 4. (Color online) Internal atomic structures on cross sections of $R = 1.7$ nm ($N = 603$) nanoparticles viewed from the [010] direction are displayed in terms of the centrosymmetry parameter. The labels (a), (b), and (c) in the picture stand for atoms having a perfect fcc crystal, surface atoms, and defects, respectively. A slip-plane glide is identified by the dislocated atoms labeled as (c) in the right nanoparticle owing to an impact at $v_{\rm coll} = 103$ m/s.

When the temperature is increased, the approximate power law in the plastic collision regime does not remain valid. Figure 3 essentially shows that the hotter nanoparticles get softer than the colder nanoparticles as expected. However, a closer look at the slope of the COR drop due to temperature rise occurs only in the range of velocity between 80 and 129 m/s. It appears that the COR at velocity higher than $v_{\rm coll} = 155$ m/s is insensitive to temperature, that is, energy loss associated with permanent deformations is not influenced by the temperature change. It is indicated that energy loss in colliding nanoparticles in the plastic collision range is seemingly tied to the degree of permanent deformation and to the corresponding deformation modes [4]. There are several mechanisms of permanent deformations of colliding or compressed nanoparticles reported elsewhere involving slip [4,31], phase transformation [9,32–35], and twinning [36,37]. Thus, an investigation on permanent deformation modes is worth pursuing for the COR drop in the particular velocity range and its temperature dependence.

Figure 4 displays deformed nanoparticles that have collided at $v_{\rm coll} = 103$ m/s, which corresponds to a mode where a single slip plane is present on the right nanoparticle. The centrosymmetry parameter [38], which can detect defects determined based on inversion symmetry, for each atom is depicted in a color gradient from red (a) to blue (b) on cross sections sliced at their centers parallel to the (010) plane. Red (a) and blue (b) designate centrosymmetric atoms and surface atoms, respectively. Pink (c) represents defects or largely displaced atoms owing to thermal motions. The aligned atoms colored in pink (c) in the right nanoparticle show the formation of a slip plane that stretches on the $(\bar{1}11)$ plane, which is one of the slip systems {111} for fcc single crystals [39]. The slip plane between the two-atom layers seen in the figure actually extends to its free surfaces.

It is found that the dislocation is nucleated at the contact surface and propagates in the $[\bar{2},\bar{1},\bar{1}]$ direction on the $(\bar{1}11)$ plane of the nanoparticle. The nanoparticles prepared here are small ($R < 10$ nm) and defect-free. Therefore, the dislocation propagation through the body of the nanoparticle is unlikely to be hindered by interactions of preexisting or induced defects such as grain boundaries [39] and twin boundaries [37,40], which generally cause hardening of materials. Hence, the slip deformation in the single crystal is inevitably extensive even at yield velocities, resulting in nanoparticles softer than polycrystalline materials [40,41] or nanoscale materials with defects [37,40,42]. Apart from the atoms lying on the slip plane and the surface, both parts drawn in red (a) remain intact. This deformation by slip is the primary deformation mechanism in the range of relatively low collision velocity, as illustrated in Fig. 3, though multiple slips and slip bands emerge when the impact gets stronger. Please note that the left nanoparticle in Fig. 4 undergoes plastic deformation only in a limited area around the contact surface. The flat surface area, which is larger than the original surface area, is formed owing to the impact as was observed in a nanocompression simulation in Ref. [36].

A high-speed collision at $v_{\rm coll} \geqslant 207$ m/s induces a different plastic deformation mode, namely twinning. Figure 5 shows snapshots viewed from two different directions that exhibit the internal atomic structures of one of the nanoparticles after collision. The nanoparticle gets squeezed in the direction parallel to the collision axis [001] and elongated in the directions perpendicular to the collision direction. Consequently, the nanoparticle is deformed like a pancake. The strong impact also alters the crystal structures, as illustrated in Figs. 5(b) and 5(c). The original atomic arrangement on a cross section displayed in Fig. 5(a), which is viewed from the $\langle 100 \rangle$ directions, turns into a new arrangement shown in Fig. 5(b). An atomic layer, for instance the layer B in the same figure, moves relative to the adjacent layer A along with a small amount of displacement from the original position. The layer C moves in the same manner relative to the layer B. This distortion process by shear stress occurs homogeneously in the right portion of the nanoparticle, which is separated by the twin boundary, a vertical solid line at the center. The mirror-symmetric arrangement is located in the left portion, giving rise to the formation of the twinning.

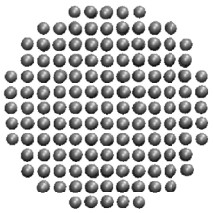

(a) Atomic arrangement of an undeformed nanoparticle in the ⟨100⟩ directions.

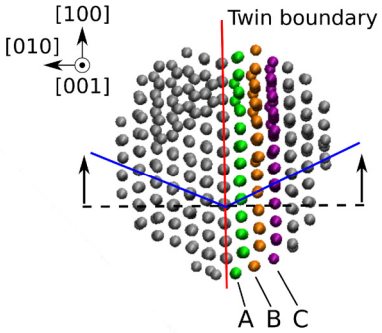

(b) Viewed from the [001] direction.

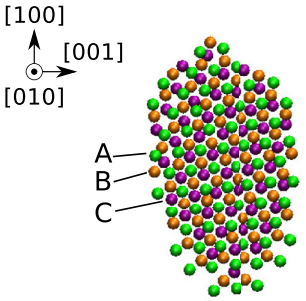

(c) Viewed from the [010] direction.

FIG. 5. (Color online) The snapshots displayed in (b) and (c) illustrate twinning deformation occurred in the $R = 1.7$ nm ($N = 603$) nanoparticle that has collided in the [001] direction. The snapshot in (a) is a cross section before collision.

The two plastic deformation modes observed in the different velocity regimes elucidate the temperature dependence in the COR. In general, slip deformation in crystals occurs at relatively low strain rate and is a thermally activated process [39], whereas twin deformation emerges at high strain rate and is not affected by temperature [43]. In fact, the COR drop seen in Fig. 3 is significant in the slip-dominant regime and is little in the twinning-dominant regime regardless of the temperature increase.

2. *Sticky nanoparticles*

Let us redefine the COR for sticky nanoparticles to consider the effect of adhesion when the nanoparticles are sufficiently close to each other. It would be challenging to experimentally measure a nanoparticle's velocity immediately before and after mutual contact. Moreover, the velocity increase caused by the attraction between nanoparticles is negligible compared with the collision velocity when it is sufficiently high [9]. The COR of sticky nanoparticles we use here is computed based on velocities of the nanoparticles outside of the range of attraction, i.e., $r_{ij} \geqslant 2.5\sigma$ in Eq. (2). The definition may be convenient to use when one compares the experimental COR to the computed COR from it.

Figure 6 shows the COR of a sticky nanoparticle of $N = 5\,481$ atoms (radius $R = 3.5$ nm), defined by Eq. (2). The adhesion strength C in the same equation for atoms in different nanoparticles is varied between 0.2 and 0.5 to create bouncy nanoparticles [6–9,44–46], which would mimic actual nanoparticles. Bouncing bismuth nanoparticles impacting on a surface were experimentally observed in Ref. [21]. When the strength C is set at 0.5, the nanoparticle is the stickiest. As a reference, the COR of the hard nanoparticle reported in Ref. [4] is shown as solid diamonds, which were fitted to a line with a slope of $\alpha = 1$ in the log-log plot.

The collisional behavior of the sticky nanoparticle impacting on the (001) facet approaches that of the hard nanoparticle as the adhesion strength C is reduced. Particularly, at the weakest adhesion $C = 0.2$ the sticky nanoparticle is more or less identical to the hard nanoparticle. This low-adhesion behavior is expected due to the weak attraction and the small size. The attraction causes the slight increase in collision velocity while the nanoparticles are approaching each other. However, this is a negligible effect since the collision velocity range of interest for the study of plastic collisions is higher than the velocity increase due to the adhesive effect [9]. This discussion is valid as long as colliding nanoparticles are sufficiently large and the adhesion is reasonably weak. The present sticky nanoparticle with $C = 0.2$ is larger in size and weaker in adhesion compared to a nearly spherical LJ nanoparticle of $N = 1055$ atoms with adhesion $C = 0.3$ colliding on a flat surface as reported by Jung [9]. The same discussion about the adhesion effect basically holds true for the departing nanoparticles, although they decelerate and their rebound velocity decreases in this case. Therefore, the weakly sticky nanoparticles behave as if they were nonadhesive nanoparticles.

The attraction is basically a surface force and determined primarily by contact area and surface energy of the contacting nanoparticles. The contact area depends strongly on the collision velocity and dramatically grows with increasing collision velocity in Refs. [4,5,9,34,47]. The contact area computed in Ref. [48] increases more rapidly than the prediction from the Hertz contact law. It indicates that the attraction would become more significant at the collision velocity where the nanoparticles are flattened and their contact surfaces are elongated. Nevertheless, the COR of the soft

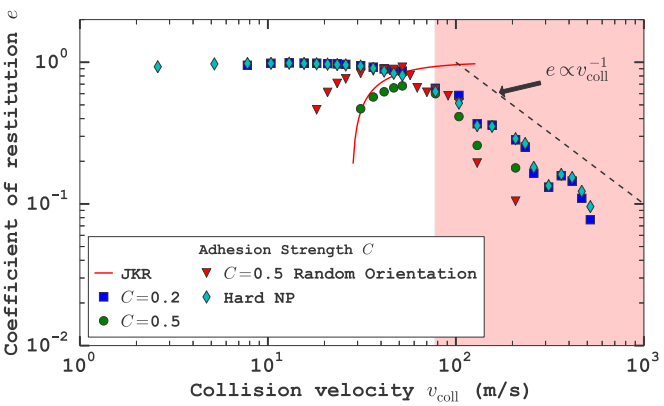

FIG. 6. (Color online) Coefficient of restitution for a sticky nanoparticle of $N = 5481$ atoms with adhesion strength C in Eq. (2). The nanoparticles collide on the {100} facets except for random orientation as noted in the legend. Plastic collision regime is shaded.

nanoparticles drops in a nearly uniform manner at every collision velocity. It suggests that the kinetic energy loss of rebounding nanoparticles due to the attraction is relatively small compared with the loss from the irreversible processes such as plastic deformation. Consequently, the CORs of the weakly adhesive nanoparticles decay at a similar rate with increasing collision velocity.

It is worth briefly mentioning the case of collision with strong adhesion. The nanoparticles with strong adhesion are prone to get stuck and never bounce back. Such coalescence occurs in highly sticky nanoparticles at $C = 0.5$ at high collision velocity. The COR that corresponds to the occurrence of coalescence is zero. Any ensemble-averaged COR at collision velocities where the nanoparticles coalesced was excluded from the plot in order to solely discuss the COR for rebounding nanoparticles. The nanoparticles at $C = 0.5$ frequently adhere to the other nanoparticles even at relatively low collision velocities, 100–300 m/s, where the nanoparticles permanently deform without the elongation of the contact surface. It indicates that the extensive plastic deformation is therefore unnecessary for the nanoparticles at this adhesion strength to adhere to the $\{100\}$ surfaces.

We have also conducted simulations for other sticky nanoparticles of $N = 603$ ($R = 1.6$ nm) and $44\,403$ ($R = 7.1$ nm) in order to investigate the effects of adhesion on the COR. We find that the fundamental behavior of the larger nanoparticles in this velocity range remains unchanged in spite of the size increase.

B. Low-velocity collision

An object that collides gently remains intact after collision. In an ideal collision, i.e., a perfectly elastic collision, the COR $= 1$. However, any kinetic energy loss arising from, for instance, viscoelasticity and creation of surface vibrations due to an impact [22], causes the COR to be less than unity. Nanoparticles are special in the sense that their COR can exceed unity when they collide at low enough velocities [4,8,9]. It indicates that the outgoing nanoparticles after collision can move faster than incoming nanoparticles. Energy transfer from the internal energy to the translational kinetic energy makes it possible for the nanoparticles to gain energy.

Here, we show the low-speed collision phenomena for the two different types of nanoparticles. The discussion on the soft nanoparticles is focused on the temperature dependence of the COR. The discussion on the sticky nanoparticles is focused on the effect of adhesion on the COR and a comparison with the COR for adhesive macroscopic spheres.

1. Soft nanoparticles

The COR of the purely repulsive soft nanoparticle colliding elastically at the collision velocity $v_{\rm coll} < 50$ m/s is shown in Fig. 3. At the lowest collision velocity $v_{\rm coll} = 2.6$ m/s, one encounters CORs that exceed unity as first reported in Refs. [8,45] and also in Ref. [34]. This superelasticity looks particularly pronounced at higher temperatures in the figure because of the correspondingly higher thermal velocities that could be transformed into the translational motion of the nanoparticles [8,45,49,50]. Apart from the superelastic collision, the COR at the lowest temperature stays near but below unity in the velocity range for elastic collision.

The COR in the elastic collision regime exhibits viscoelastic behavior that is characterized by a monotonically decreasing COR with increasing rebound velocity because of the loss of energy along with temperature rise. The viscoelasticity of two spherical particles in contact is described by two nonlinear forces, that is, the Hertz contact force and a nonlinear damping force [51,52]. The mathematical models can account for velocity-dependent CORs of macroscopic spheres obtained from experiments in Refs. [51,53–56]. The viscoelasticity of the present nanoparticles at $T = 2.4$ K is vanishingly small, which is displayed in Fig. 3 as the nearly velocity-independent COR. As the temperature increases, the COR drop becomes more prominent and extended toward the lower collision velocity.

There are a number of viscoelastic models proposed for colliding spheres based on continuum theory, and their model parameters are determined from experimental data. Although it would be interesting to see what model is suitable for the present nanoparticles, since our CORs obtained at the widely varied temperatures show significant variations, it is not worth estimating reliable temperature-dependent model parameters for our data.

The low temperature behavior of the COR, being almost constant and close to unity, may look inconsistent with an obvious velocity-dependent COR of two colliding nanoparticles at the same temperature $T = 2.4$ K presented by Kuninaka and Hayakawa in Ref. [8]. The nanoparticles prepared by the authors [8] had a density much lower than they should have had as reported in a subsequent work in Ref. [33]. Such low-density nanoparticles could be "fluffy," and kinetic energy associated with the translational motion of the fluffy nanoparticles presumably dissipates more than that of dense nanoparticles [54]. For further confirmation, we made fluffy and weakly adhesive nanoparticles with an interatomic repulsive energy reduced to 60% of the original repulsive energy $4\epsilon(\sigma/r_{ij})^{12}$ and $C = 0.2$ in Eq. (2). We find that the COR of our elastically colliding fluffy nanoparticles falls with a greater negative slope if the velocity is neither too low nor too high, which appears to be consistent with the COR exhibited in Ref. [8].

2. Sticky nanoparticles

The sticky nanoparticle's COR at several adhesion strengths C is displayed in Fig. 6. We focus on the elastic collision regime where the velocity range is approximately between 2 and 50 m/s. The adhesion affects the COR a great deal when the strength C is high. The COR at a low adhesion strength, $C = 0.2$, is identical to the CORs of the hard nanoparticles. This behavior for the low-speed nanoparticles is similar to that for the high-speed nanoparticles. However, the underlying mechanisms of the COR drops are quite different.

For the low-speed collisions, the contact area remains unchanged [57] during collision. What reduces the rebound velocity is entirely the attraction on the contact surface. The energy loss in the kinetic energy originating from the attraction becomes appreciable, particularly at $C = 0.5$, as the collision velocity is reduced.

This COR behavior of sticky nanoparticles, which declines at high adhesion strengths with decreasing velocity, may be described by a function of the velocity. For macroscopic adhesive spheres, their velocity-dependent COR may be described by the JKR theory. The JKR theory incorporates adhesion energy acting on the contact surface of the spheres in the Hertzian contact theory. We apply this theory to the slowly colliding sticky nanoparticles in order to obtain the behavior of the COR. There are many suggested models that can describe adhesive contact [58], but for a comparison with the nanoparticle's COR the JKR theory may be suited for the present nanoparticles that collide on the large faceted surface.

The COR of such adhesive spheres is given with a sticking velocity v_s in Ref. [59] by

$$e = \left[1 - \left(\frac{v_s}{v_{\rm coll}}\right)^2\right]^{1/2}. \tag{4}$$

The sticking velocity v_s is a critical velocity below which spheres get stuck by adhesion and is expressed in Eq. (5):

$$v_s = \left(\frac{14.18}{m^*}\right)^{1/2}\left(\frac{\gamma^5 R^{*4}}{E^{*2}}\right)^{1/6}, \tag{5}$$

where reduced radius $R^* = R/2$ and reduced Young's modulus $E^* = E/[2(1-\nu^2)]$. The quantities used here R, E, and ν are radius, Young's modulus, and Poisson's ratio of the nanoparticles, respectively. The velocity is obtained by taking into account that the only energy loss during collision is the energy spent to separate the contacting surfaces. We may be able to apply the JKR theory to the sticky nanoparticles by assuming that the nanoparticles are perfect spheres of radius $R = 3.5$ nm. The theoretical sticking velocity for the nanoparticle of $N = 5481$ calculated from the continuum theory-based Eq. (5) is 27 m/s. The surface energy $\gamma = 0.044568\,\mathrm{J/m^2}$ of the (100) surface of solid argon at $T = 0$ K [60]. The modulus $E^* = 1.36 \times 10^9$ Pa with $\nu = 0.347$ [61]. The solid red curve in Fig. 6 is a theoretical COR computed from Eq. (4) with the sticking velocity v_s obtained above.

It seems that the COR of the sticky nanoparticles is approaching the theoretical COR as predicted by the JKR theory. The COR at the strong adhesion strength $C = 0.5$ falls off gradually with decreasing velocity. Their behavior looks similar to the JKR's. The result suggests that the JKR theory may be valid for the nanoparticles with the strong adhesion strengths that collide on the {100} surfaces. In contrast to the strong adhesion cases, the weakly adhesive nanoparticles display no or a small drop in their CORs for $C = 0.2$–0.4 and the abrupt occurrence of sticking nanoparticles observed at around $v_{\rm coll} \sim 10$ m/s.

It is surprising that the JKR theory is seemingly pertinent to nanoscale particles that possess large facets. The JKR theory relies on the Hertzian theory in which the contact areas of two elastic spheres that vary in accordance with compression is assumed. Thus, we carry out a further test on one of the strong adhesion cases in order to assess the validity of the JKR theory at nanoscale. The size dependence of the sticking velocity for the nanoparticles at adhesion strength $C = 0.5$ is displayed in Fig. 7. The sticking velocity for the JKR spheres decays with $R^{-5/6}$, which is contributed from both $R^{4/6}$ and $m^{-1/2} \propto R^{-3/2}$ in Eq. (5). The nanoparticle's sticking velocity appears to scale as the JKR spheres do. However, there are only three data points for the nanoparticles, and hence further simulations with different sizes are desirable for confirmation of the size dependence of the sticking velocity.

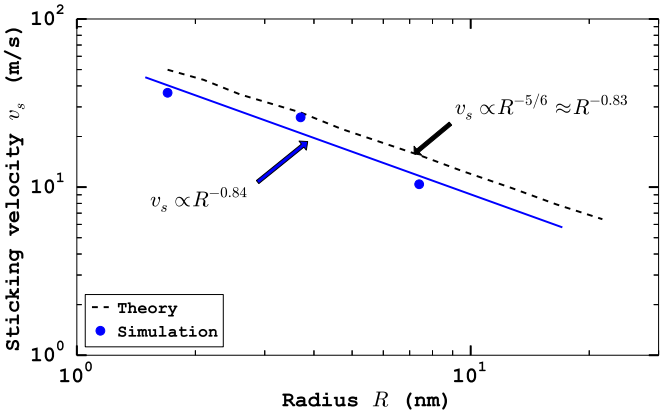

FIG. 7. (Color online) Size dependence of sticking velocity v_s for the strongly sticky nanoparticle colliding on the {100} faceted surfaces at adhesion strength $C = 0.5$. The dashed line is the prediction from the JKR theory.

We have thus far let the sticky nanoparticles collide on their facets. Figure 6 also presents the COR for randomly oriented sticky nanoparticles at $C = 0.5$ to examine the role of surface roughness. Edge-edge collisions of the randomly orientated nanoparticles occur more frequently than facet-facet collisions. The edge-edge collision is expected to reduce the contact area between two nanoparticles compared with the facet-facet collision case. The COR for the random orientation in Fig. 6 that shifts toward the lower collision velocity demonstrates that the nanoparticles become less sticky as expected.

IV. CONCLUSION

In this molecular dynamics study, we have presented the collisional properties of two types of nanoparticles, soft nanoparticles and sticky nanoparticles, colliding at velocities ranging between the elastic and plastic collision regimes.

In the plastic collision regime, both the nanoparticles can be described by the coefficient of restitution $e \propto v_{\rm coll}^{-\alpha}$ with $\alpha \sim 1$. This result is consistent with the extreme softening found in the purely repulsive hard nanoparticles when temperature is low enough, although bounciness of the soft nanoparticle and the sticky nanoparticle was reduced further. The crystal structure analyses revealed two distinct plastic deformation modes: slip and twinning. We find that the defect-free crystals allow the dislocations to propagate in the entire nanoparticle and consequently it causes the colliding nanoparticles to be softer than their macroscopic equivalents. The considerably deformed and elongated contact surfaces increased the attraction and led to sticker nanoparticles.

In the elastic collision regime, the velocity-dependent collisional behavior of the sticky nanoparticle is similar to

that of the macroscopic counterpart predicted by the Johnson-Kendall-Roberts elastic contact theory when adhesion strength of the nanoparticle is sufficiently strong. The presence of facets on nanoparticles' surface increases the chance of adhesion.

ACKNOWLEDGMENTS

We thank the US Army Research Office for partial support of the research reported here. We thank Professor H. Kuninaka and Professor H. Hayakawa for their helpful correspondences.

[1] T. Rodriguez-Suarez, J. F. Bartolomé, and J. S. Moya, J. Eur. Ceram. Soc. **32**, 3887 (2012).
[2] W. W. Gerberich, W. M. Mook, C. R. Perrey, C. B. Carter, M. I. Baskes, R. Mukherjee, A. Gidwani, J. Heberlein, P. H. McMurry, and S. L. Girshick, J. Mech. Phys. Solids **51**, 979 (2003).
[3] D. Hull and D. J. Bacon, *Introduction to Dislocations*, Vol. 257 (Pergamon Press Oxford, London, 1984).
[4] Y. Takato, S. Sen, and J. B. Lechman, Phys. Rev. E **89**, 033308 (2014).
[5] S. Kim, Phys. Procedia **34**, 66 (2012).
[6] A. Awasthi, S. C. Hendy, P. Zoontjens, and S. A. Brown, Phys. Rev. Lett. **97**, 186103 (2006).
[7] A. Awasthi, S. C. Hendy, P. Zoontjens, S. A. Brown, and F. Natali, Phys. Rev. B **76**, 115437 (2007).
[8] H. Kuninaka and H. Hayakawa, Phys. Rev. E **79**, 031309 (2009).
[9] S.-c. Jung, D. Suh, and W.-s. Yoon, J. Aerosol Sci. **41**, 745 (2010).
[10] H. Gleiter, Prog. Mater. Sci. **33**, 223 (1989).
[11] M. Vergeles, A. Maritan, J. Koplik, and J. R. Banavar, Phys. Rev. E **56**, 2626 (1997).
[12] D. J. Quesnel, D. S. Rimai, and L. P. Demejo, J. Adhesion **67**, 235 (1998).
[13] D. S. Rimai, D. J. Quesnel, and A. A. Busnaina, Colloids Surf. A **165**, 3 (2000).
[14] J. M. Carrillo, E. Raphael, and A. V. Dobrynin, Langmuir **26**, 12973 (2010).
[15] J. M. Carrillo and A. V. Dobrynin, Langmuir **28**, 10881 (2012).
[16] A. Chokshi, A. Tielens, and D. Hollenbach, Astrophys. J. **407**, 806 (1993).
[17] C. Dominik and T. A. G. G. M., Astrophys. J. **480**, 647 (1997).
[18] J. Blum, Res. Astron. Astrophys. **10**, 1199 (2010).
[19] H. Tanaka, K. Wada, T. Suyama, and S. Okuzumi, Prog. Theor. Phys. Suppl. **195**, 101 (2012).
[20] K. Johnson, K. Kendall, and A. Roberts, Proc. R. Soc. Lond. A, Math. Phys. Sci. **324**, 301 (1971).
[21] A. Ayesh, S. Brown, A. Awasthi, S. Hendy, P. Convers, and K. Nichol, Phys. Rev. B **81**, 195422 (2010).
[22] K. Johnson, *Contact Mechanics* (Cambridge Univiersity Press, Cambridge, 1987).
[23] C. Thornton, J. Appl. Mech. **64**, 383 (1997).
[24] J. D. Weeks, D. Chandler, and H. C. Andersen, J. Chem. Phys. **54**, 5237 (1971).
[25] S. Nosé, J. Chem. Phys. **81**, 511 (1984).
[26] W. G. Hoover, Phys. Rev. A **31**, 1695 (1985).
[27] J. D. Honeycutt and H. C. Andersen, J. Phys. Chem. **91**, 4950 (1987).
[28] A. Rytkönen, S. Valkealahti, and M. Manninen, J. Chem. Phys. **106**, 1888 (1997).
[29] S. Plimpton, J. Comput. Phys. **117**, 1 (1995).
[30] W. Humphrey, A. Dalke, and K. Schulten, J. Mol. Graphics **14**, 33 (1996).
[31] K. Saitoh and Y. Yonekawa, J. Adv. Mech. Des. Sys. Man. **4**, 405 (2010).
[32] P. Valentini and T. Dumitrica, J. Nano Res. **1**, 31 (2008).
[33] K. Saitoh, A. Bodrova, H. Hayakawa, and N. V. Brilliantov, Phys. Rev. Lett. **105**, 238001 (2010).
[34] L. Han, Q. An, S. Luo, and W. Goddard, Mater. Lett. **64**, 2230 (2010).
[35] N. Zhang, Q. Deng, Y. Hong, L. Xiong, S. Li, M. Strasberg, W. Yin, Y. Zou, C. R. Taylor, G. Sawyer, and Y. Chen, J. Appl. Phys. **109**, 063534 (2011).
[36] J.-J. Bian and G.-F. Wang, J. Compt. Theor. Nanos. **10**, 2299 (2013).
[37] J. Bian, X. Niu, H. Zhang, and G. Wang, Nanoscale Res. Lett. **9**, 1 (2014).
[38] C. L. Kelchner, S. Plimpton, and J. Hamilton, Phys. Rev. B **58**, 11085 (1998).
[39] W. F. Hosford, *Mechanical Behavior of Materials* (Cambridge University Press, Cambridge, 2005).
[40] C. Deng and F. Sansoz, Nano Lett. **9**, 1517 (2009).
[41] U. Kocks, Acta Metall. **8**, 345 (1960).
[42] J. Wang, F. Sansoz, J. Huang, Y. Liu, S. Sun, Z. Zhang, and S. X. Mao, Nat. Commun. **4**, 1742 (2013).
[43] H. S. Park, K. Gall, and J. A. Zimmerman, J. Mech. Phys. Solids **54**, 1862 (2006).
[44] A. Awasthi, e-J. Surf. Sci. Nanotech. **6**, 307 (2008).
[45] H. Kuninaka and H. Hayakawa, Prog. Theor. Phys. Suppl. **178**, 157 (2009).
[46] A. Awasthi, S. C. Hendy, and S. A. Brown, Math. Mech. Solids **15**, 771 (2010).
[47] M. Suri and T. Dumitrică, Phys. Rev. B **78**, 081405 (2008).
[48] S.-C. Jung, J.-G. Bang, and W.-s. Yoon, J. Aerosol Sci. **50**, 26 (2012).
[49] H. Kuninaka and H. Hayakawa, Phys. Rev. E **86**, 051302 (2012).
[50] R. Murakami and H. Hayakawa, Phys. Rev. E **89**, 012205 (2014).
[51] G. Kuwabara and K. Kono, Jpn. J. Appl. Phys. **26**, 1230 (1987).
[52] N. V. Brilliantov, F. Spahn, J. M. Hertzsch, and T. Pöschel, Phys. Rev. E **53**, 5382 (1996).
[53] F. G. Bridges, A. Hatzes, and D. Lin, Nature **309**, 333 (1984).
[54] A. P. Hatzes, F. G. Bridges, and D. Lin, Mon. Not. R. Astron. Soc. **231**, 1091 (1988).
[55] K. D. Supulver, F. G. Bridges, and D. N. C. Lin, Icarus **113**, 288 (1995).
[56] L. Labous, A. D. Rosato, and R. N. Dave, Phys. Rev. E **56**, 5717 (1997).
[57] Y. Takato and S. Sen (unpublished).
[58] J. Tomas, in *International Symposium on Particles on Surfaces: Detection, Adhesion and Removal*, Vol. 8, edited by K. L. Mittal (VSP, Utrecht, 2003), pp. 183–229.
[59] C. Thornton and Z. Ning, Powder Technol. **99**, 154 (1998).
[60] D. Maugis, *Contact, Adhesion and Rupture of Elastic Solids*, Vol. 130 (Springer Science & Business Media, Berlin, 2000).
[61] D. J. Quesnel, D. S. Rimai, and L. P. DeMejo, Phys. Rev. B **48**, 6795 (1993).